How electrons still guard the space: Electron number distribution functions based on QTAIM∩ELF intersections

Daniel Barrena-Espés,[1] Julen Munárriz,[2] and Ángel Martín Pendás[1]

[1)]*Departamento de Química Física y Analítica, Universidad de Oviedo, 33006 Oviedo, Spain.*

[2)]*Departamento de Química Física and Instituto de Biocomputación y Física de Sistemas Complejos (BIFI), Universidad de Zaragoza, 50009 Zaragoza, Spain.*

(*Electronic mail: ampendas@uniovi.es)

(*Electronic mail: julen@unizar.es)

(Dated: 14 March 2024)

Despite the importance of the one-particle picture provided by the orbital paradigm, a rigorous understanding of the spatial distribution of electrons in molecules is still of paramount importance to chemistry. Considerable progress has been made following the introduction of topological approaches, capable of partitioning space into chemically meaningful regions. They usually provide atomic partitions, for example through the attraction basins of the electron density in the quantum theory of atoms in molecules (QTAIM), or electron-pair decompositions, as in the case of the electron localization function (ELF). In both cases, the so-called electron distribution functions (EDF) provide a rich statistical description of the electron distribution in these spatial domains. Here we take the EDF concept to a new fine-grained limit by calculating EDFs in the QTAIM∩ELF (QEI) intersection domains. As shown in AH_n systems based on main group elements, as well as in the CO, NO, and BeO molecules, this approach provides an exquisitely detailed picture of the electron distribution in molecules, allowing for a insightful combination of the distribution of electrons between Lewis entities (such as bonds and lone pairs) and atoms at the same time. Besides mean-field calculations, we also explore the impact of electron correlation through HF, DFT (B3LYP) and CASSCF calculations.

I. INTRODUCTION

Understanding the nature of the chemical bond, a no-concept which needs not to be invoked to run the everyday more common multi-thousand atom simulations that fill scientific journals, but without which chemists feel naked in a calculable yet non-understandable quantum mechanical world is still a relevant enterprise that elicits quite a number of interesting discussions.[1] Aside from specific spiky chemical-like debates, e.g. on the existence of a quadruple bond in the ground state of the dicarbon molecule,[2–4] the electrostatic or not electrostatic nature of an ever-growing zoo of new non-covalent interactions like pnictide, chalcogen, or halogen bonds,[5] or the need to define a third charge-shift category of bonds beyond the covalent and ionic ones,[6] and also away from the physical debate regarding the kinetic or potential energy driving forces behind cohesion,[7] a rather uncontested principle emerges when we examine the ashes that remain after the fires. Electron delocalization, dressed in different disguises, lies at the root of bonding.[8]

As expected, much work has been gathered around the role of localization and delocalization in all kinds of phenomena.[9] Focusing on spatial descriptions, closer to chemistry than those based on the momentum representation, the contemporary theoretical or computational chemist can now choose among a rather large number of local, semi-local or integrated quantities: localization (LI) and delocalization (DI) indices,[10] based on the electron, ρ, and pair, ρ_2, densities, or the electron localization function (ELF),[11] the localized orbital locator (LOL),[12] the electron localizability indicator (ELI)[13] and maximum probability domains (MPDs),[14–16] to name just a few. When a local scalar field is involved (as with the ρ, ELF, LOL, or ELI functions) the toolkit of the so-called quantum chemical topology (QCT)[17] is also typically used to provide an exhaustive partition of the space into attraction basins. In this way, atomic, or chemically meaningful subatomic regions associated with cores, bonds, or lone-pairs are obtained in an orbital-invariant manner.

The theoretical roots of these descriptors differ, traversing from the curvature of the Fermi hole to the excess kinetic energy of a fermionic system with respect to that of a bosonic one. In all cases, the indices can be related to the population fluctuations exhibited by the electron distribution. After all, in a world with indistinguishable electrons, spatial localization/delocalization must ultimately be linked to Born's probability, thus to the statistics of the electron distribution itself. This is rather obvious in the case of LIs and DIs, obtained after integrating the two coordinates in the exchange-correlation density over either the same or different finite spatial domains, respectively. They are immediately related to the variance and covariance of appropriately defined marginal

probabilities of the electron populations.[18] Actually, it has been shown that the standard Wiberg-Mayer two-center bond orders,[19,20] as well as their multi-center counterparts,[21] are just measures of these fluctuations, appropriately condensed through the cumulant moments of the many-center probability distributions.

Sure enough, if many of our daily chemical indices are no more than statistical moments of a probability distribution, examining the distribution itself should be an interesting endeavor. A rather general methodology to obtain them has already been devised.[22] In short, given an externally provided division of $\mathbb{R}^3$ into a set of m non-overlapping regions, $\Omega_1,\ldots,\Omega_m$, one can obtain the probability of finding a given partition of the N electrons of a system $n_1,n_2,\ldots,n_m$, $\sum_{i=1}^{m} n_i = N$ such that n_1 electrons are found in Ω_1, n_2 in Ω_2, etc. The full set of all these $p(n_1,n_2,\ldots,n_m)$ probabilities is called the electron distribution function (EDF).[23] Using the atomic regions given by the quantum theory of atoms in molecules (QTAIM),[24] EDFs provide a wealth of information about the electronic structure of a system from which all the above-mentioned multi-center bond orders are immediately obtained. Far beyond, they have been shown to give an exquisitely detailed picture of chemical bonding in standard as well as exotic situations that is not available otherwise.[25] Despite their apparent complexity, the recognition of common bonding descriptors such as the delocalization index, as the covariance of a two-domain EDF has allowed understanding, predicting, and finding cases where it is negative or surpasses its traditionally allowed values, discovering potentially completely new bonding regimes.[26] Surprisingly, EDFs have not been consistently explored so far in the case of topological partitions coming from fields other than the electron density. In the case of the ELF or of maximum probability domains, for instance, only one-basin variances and their associated single-region probabilities, $p(n)$, as well as two-basin covariances, have been obtained and discussed routinely.[27] The availability of single-region probabilities is related to the existence of a fast, recursive algorithm devised by E. Cancès valid only for one-determinant wavefunctions.[14] Not much is known about multi-center EDFs, particularly in highly correlated cases, although interesting works[28,29] have been published about the relation between EDFs and aromaticity in Hubbard models of maximum probability domains.

It is our purpose to fill this gap with this contribution. To that end, we have decided to use as thinner a decomposition of $\mathbb{R}^3$ as possible without sacrificing simplicity. A simple solution is to intersect atomic basins with electron-pair ones. This has been done several times before. For instance, QTAIM and ELI intersections have provided further insight into the chemical bonding in intermetallics.[30] QTAIM$\cap$ELF intersections (QEI), originally proposed by Raub and Jansen,[31]

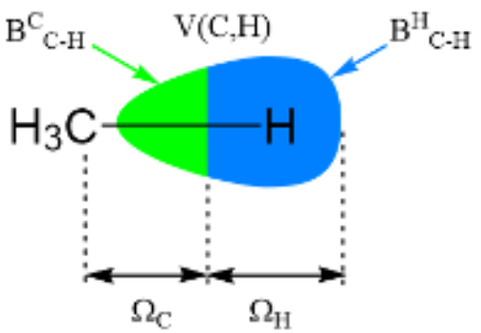

FIG. 1. Simplified QEI partition scheme for a hydrogenic V(C,H) basin, which represents the C-H bond, of the methane molecule.

have also been reported as a means to correlate electronegativity scales with each of the atomic shares of an ELF bonding pair population.[32–34] In the QEI approach, monosynaptic ELF basins like cores C(A) or lone pairs V(A), belonging entirely to a given QTAIM atomic domain A, are not altered by QTAIM intersections, but polysynaptic ELF basins are split into a number of sub-regions depending on their synapticity.[33] Thus, for a general disynaptic ELF attractor V(A,B), related to an A-B bond, two sub-domains arise, one for the portion of the ELF basin contained within Ω_A, and the other for its equivalent Ω_B counterpart (an schematic representation involving a hydrogenic V(C,H) basin is shown in Fig. 1). This provides a very detailed decomposition of the electron population into chemically meaningful objects: atomic cores and lone pairs, and bonding electrons separated into atomic contributions. Given its introductory purpose, we have examined relatively simple albeit chemically relevant examples, trying to show what new insights this approach offers that are hidden in other analyses.

We start by summarizing succinctly the theoretical framework leading to the QEI partition and the electron distribution functions. Next, we explore the statistical insights offered by EDF analysis in various hydrides, considering both QTAIM and ELF partitions. Subsequently, we apply the topological partition offered by QEI to obtain a more comprehensive description of the bonding. Hereinafter, the study is extended to the more interesting CO, BeO and NO diatomic species reproducing the same procedure as for the hydrides. Finally, we present our future prospects and draw conclusions.

II. METHODOLOGICAL FRAMEWORK

A. Real Space Partitions

1. The QTAIM partitioning scheme

The QTAIM of Bader and coworkers,[24] likely the first topological approach to chemical bonding, is based on the topology induced in $\mathbb{R}^3$ by the attraction basins provided by the gradient of the electron density, $\nabla\rho(\boldsymbol{r})$. Due to Kato's cusp theorem,[35] $\rho(\boldsymbol{r})$ around a nucleus A is homeomorphic (topologically equivalent) to a maximum, and the physical space becomes the union, in general, of a set of atomic domains, Ω_A. Thanks to the local zero-flux condition satisfied by points at the separatrices between atomic domains, $\nabla\rho(\boldsymbol{r})\cdot n = 0$, where n is the normal vector to the separatrix surface at $\boldsymbol{r}$,[24] the QTAIM atomic basins satisfy a large number of so-called atomic theorems.[24] Integrating operator densities over atomic domains gives rise to atomic expectation values.

2. The Electron Localization Function

The exclusion principle has been used many times as a guide to define localization measures. Since antisymmetry forces the same-spin pair density, $\rho_2^{\sigma\sigma}(\boldsymbol{r},\boldsymbol{r}')$, to vanish whenever $\boldsymbol{r} = \boldsymbol{r}'$, the conditional same-spin pair density, $P^{\sigma\sigma}(\boldsymbol{r},\boldsymbol{r}+\boldsymbol{s}) = \rho_2^{\sigma\sigma}(\boldsymbol{r},\boldsymbol{r}+\boldsymbol{s})/\rho(\boldsymbol{r})$ behaves parabolically with $|\boldsymbol{s}|$. Its spherically averaged curvature determines how large the region in which an electron excludes another of its same spin is, thus how localized the initial electron can be considered to be. Defining $D_\sigma = \frac{1}{2}\nabla_s^2 P^{\sigma\sigma}(\boldsymbol{r},\boldsymbol{r}+\boldsymbol{s})\Big|_{s=0}$, and scaling this value with respect to its equivalent for a homogeneous electron gas at the mean-field level, Becke and Edgecombe[11] defined the ELF kernel $\chi(\boldsymbol{r}) = D_\sigma/D_\sigma^0$ and, after a Lorenztian scaling to remap the kernel into the $[0,1]$ range, came to the following ELF ($\eta(\boldsymbol{r})$) definition,

$$\eta(\boldsymbol{r}) = \left(1+\chi^2(\boldsymbol{r})\right)^{-1}. \tag{1}$$

Given the great success of the ELF in computational chemistry,[36–39] many efforts have been made to expand its meaning beyond the mean-field approximation. For instance, the ELF admits an interpretation independent of the curvature of the Fermi hole in terms of the Fermionic excess kinetic energy density.[40,41] This allows its use in standard Kohn-Sham density functional theory (DFT).[13,42] Similarly, extensions to explicitly correlated descriptions have been proposed

by Dobson[43], Silvi[44], and Matito[45] by using directly correlated pair densities, although all these authors built the correlated ELF kernel with the standard electron gas scaling:

$$\chi(\boldsymbol{r}) = \frac{\nabla_s^2 \rho_2^{\alpha\alpha}(\boldsymbol{r}, \boldsymbol{r}+\boldsymbol{s})\big|_{s=0} + \nabla_s^2 \rho_2^{\beta\beta}(\boldsymbol{r}, \boldsymbol{r}+\boldsymbol{s})\big|_{s=0}}{2c_F \rho^{8/3}(\boldsymbol{r})}, \tag{2}$$

where c_F is Fermi's constant. Here we will use both single- or pseudo-single-determinant and correlated ELF definitions depending on the level of calculation selected.

3. The QTAIM∩ELF intersection

As stated before, any monosynaptic core or lone-pair ELF basin will, almost always, remain unaltered when intersected with QTAIM domains, while polysynaptic basins will split into several smaller QEI regions. Since we will be dealing mainly with disynaptic basins (including, as it is customarily done, the V(A,H) bond basins in this category), we will adopt the following nomenclature: $\mathrm{V(A,B)} \equiv \mathrm{B}^{\mathrm{A}}_{\mathrm{A\text{-}B}} \cup \mathrm{B}^{\mathrm{B}}_{\mathrm{A\text{-}B}}$. That is, as a consequence of the intersection with a given QTAIM domain, V(A,B) bond ELF basin is divided into two new domains, $\mathrm{B}^{\mathrm{A}}_{\mathrm{A\text{-}B}}$ and $\mathrm{B}^{\mathrm{B}}_{\mathrm{A\text{-}B}}$, which can be associated to the fraction of the original basis belonging to atoms A and B, respectively (see Fig. 1).

B. Electron distribution functions

The field of chemical bonding has traditionally been divided into two loosely related sides: an electron accounting perspective that tracks the distribution of electrons, which has given rise to concepts such as atomic populations or bond orders, and an energetic perspective that provides the notion of bond strength. The limit of electron accounting techniques in real space is probably reached when we acquire knowledge about the probability $p(n_1, n_2, \ldots, n_m)$ of finding a given partition of the $N = n_1 + n_2 + \ldots n_m$ electrons of a system into a set of m spatial regions or domains $\Omega_1, \Omega_2, \ldots, \Omega_m$ that fill the space ($\bigcup_{i=1}^{m} \Omega_i = \mathbb{R}^3$). These so-called *electron distribution functions* (EDFs) were coined by Francisco *et al*[46]. If a $\Psi(1,N)$ wave function describes the N-electron system, then the probability of finding n_1 electrons in the Ω_1 domain, n_2 in Ω_2, ..., n_m in Ω_m (i.e., the multidimensional domain D) becomes

$$p(n_1, n_2, ..., n_m) = \frac{N!}{n_1! n_2! ... n_m!} \int_D |\Psi|^2 d\boldsymbol{r}_1 d\boldsymbol{r}_2 ... d\boldsymbol{r}_N. \tag{3}$$

In the simplest situation where space is divided into two regions, Ω with n electrons, and Ω' with $N-n$ electrons, and the system is described as a single determinant built from spinorbitals χ_i, a clever recursive algorithm developed by Cancès and coworkers[14] allows for a straightforward determination of $p(n,N-n)$ once the domain overlap matrix (DOM)

$$S_{ij}^{\Omega} = \int_{\Omega} \chi_i^*(\boldsymbol{r})\chi_j(\boldsymbol{r})d\boldsymbol{r} \tag{4}$$

is known. The computation of multi-domain EDFs or even the calculation of two-domain probabilities for multiconfigurational wavefunctions is considerably more demanding, although some algorithms have been proposed for this task.[22,47] In every case DOMs obtained for the full set of partially occupied orbitals are the only raw material needed to obtain the EDF.

We note in passing that the complete EDF of a system typically contains an astronomically large number of components, since the number of partitions of N, N_S scales combinatorially with the number of electrons and the number of domains: $N_S = (N+m-1)!/(N!(m-1)!)$. Knowledge of the EDF provides easy access to any electron counting average, thus many magnitudes playing a crucial role in the chemical narrative.[22,23,48] This is the case of, for example, the average electron population of a fragment, which is directly given by

$$\langle n_A \rangle = \int_{\Omega_A} \rho(\boldsymbol{r})d\boldsymbol{r} = \sum_{n_A} n_A p(n_A) \tag{5}$$

III. COMPUTATIONAL DETAILS

Geometry optimizations were performed at the Density Functional Theory (DFT) level, by means of the GGA hybrid B3LYP[49] functional, as implemented in the Gaussian16[50] package, in conjunction with the Ahlrichs triple-zeta def2-TZVP[51] basis sets.

Several levels of theory were considered for the calculation of the wave functions (required for the topological space partition and EDF analysis) at the DFT-optimized geometries. For second-row AH_n systems, they were obtained at Hartree-Fock (HF), DFT, and CASSCF levels, while only DFT and CASSCF were considered for third-row-based systems; the wave function of fourth-row analogues was computed only at the DFT level. HF and DFT wave functions were calculated by using the Gaussian16 suite, while CASSCF calculations (CAS[i, j] in the following, where i is the number of electrons and j the number of orbitals included in the active space), were obtained from the GAMESS[52] package. The active space composition for the CASSCF calculations is provided in the Supporting Information (Table S1). The CO, BeO and NO molecules were computed at

CAS and B3LYP levels of theory. In the particular case of NO, given that it is a doublet in the ground state, unrestricted B3LYP was performed.

Both the QTAIM and ELF partitions were obtained by means of the TopMod package[53]. When working with multi-determinant (CASSCF) wave functions, the ELF was calculated by using a modified version of the original TopMod code, which is publicly available[54]. The EQI was obtained by our in-house code, which is available upon request. The domain overlap matrices required for the EDF calculation were obtained from the TopMod package. Finally, the electron distribution functions were computed with the EDF program[47].

IV. RESULTS AND DISCUSSION

A. EDFs on QTAIM basins

To fully understand the wealth of information contained in the QEI partition, it is necessary to consider the parent results in the case of standard QTAIM and ELF decompositions. Therefore, we begin by summarizing the EDFs within the 2-basin QTAIM atomic partition, which will later be completed by the multi-basin EDF analysis encompassing the most meaningful scenarios.

As introduced by some of us in earlier works[22,23,46,48] when using QTAIM atomic basins, each partition of the N electrons in the molecule can be referred to as a real space resonance structure (RSRS). Each RSRS assigns a specific number of electrons to each atom (which may include zero), and the relative distribution of different RSRSs provides a chemically intuitive representation of chemical bonding. A system characterized by a broad RSRS distribution (with many substantial probabilities) may be associated with higher covalency due to increased electron delocalization. Conversely, a reduced number of structures or a single high-probability structure that does not coincide with neutral atoms results in a narrower distribution, indicating highly polar bonding regimes where electrons tend to localize around specific centers. The shift of the highest probability peak with respect to the neutral RSRS, i.e. the one where all spatial regions have the same number of electrons as the neutral atoms, intuitively shows variations in electronegativity: the most electronegative regions attract more electrons.

Let n_A^0 be the number of electrons of Ω_A in the neutral distribution and n_A be the actual number of electrons of Ω_A in a given RSRS. Then $n_A - n_A^0$ will take negative values in situations where A has lost electrons, i.e, in $A^{\delta+}(H_n)^{\delta-}$ structures in chemical jargon (for AH_n systems), while it will

take positive values when A gains electrons with respect to its neutral state, i.e. in the case of an $A^{\delta-}(H_n)^{\delta+}$ polarization.

Before delving into the results, a few words about notation are due. To ensure a fair and consistent comparison between the various systems under consideration , where A atoms in the considered hydride systems may belong to different rows of the periodic table and thus have different numbers of electrons in their inner shells, we report as n_A the sum of their ns and np valence shell electrons. Thus, neutral Li, Na, and K are all labeled as $n_A = 1$ systems, while neutral O, S, and Se are identified with $n_A = 6$, just to mention some examples.

The 2-basin EDFs for second, third, and fourth-row AH_n systems are provided in Fig. 2. Note that the space has been divided into Ω_A (the basin that corresponds to atom A) and $\mathbb{R}^3 - \Omega_A$ (that is, the remaining space, which encompasses all the hydrogen atoms).

While the discussion of second-row systems has been previously addressed by some of us[46], – altough with a different methodology – a brief description of the main findings are included here to ensure a comprehensive examination and to facilitate a clearer understanding of the results derived from QEI partitions. In general, the systems can be divided into three groups according to the nature of the A-H bond (see Fig. 2a). The first group includes LiH, BeH_2, and BH_3, which are characterized by the low electronegativity (compared to hydrogen) of the central atoms. This naturally leads to dominant RSRSs in which the A atom loses electrons (relative to the neutral state), as clearly shown by the RSRS peaks at $[Li^+H^-]$, $[Be^{2+}(H_2)^{2-}]$, and $[B^{2+}(H_3)^{2-}]$. Note also that the higher the ionic character of the A-H bond, the narrower the RSRS distribution and the higher the weight of the main RSRS. Thus, as the bond polarity decreases from LiH to BH_3, the EDF becomes broader.

The second group corresponds to almost *pure* covalent bonds and finds CH_4 as its only representative. It has a main RSRS with $n_A = n_A^0$. Such a system is characterized as the most covalent, as evidenced by the relatively low probability (0.274) of the main RSRS, $[C^0(H_4)^0]$, the neutral one, and a wide, almost symmetric RSRS distribution.

The last set of systems corresponds to molecules with opposite polarity, i.e. where the electron distribution in the bond is shifted towards the A atom: NH_3, H_2O, and HF. The probability trend nicely shows how the electronegativity increases from N to F at the expense of the covalent character of the A-H bond. In fact, the main RSRS corresponds to partitions in which the A atom gains additional electrons from H atoms: $[N^-(H_3)^+]$, $[O^{2-}(H_2)^{2+}]$ and $[F^-H^+]$, and the RSRS distribution sharpens from NH_3 to HF (from 6 relevant distributions to 4 and 3, respectively), the

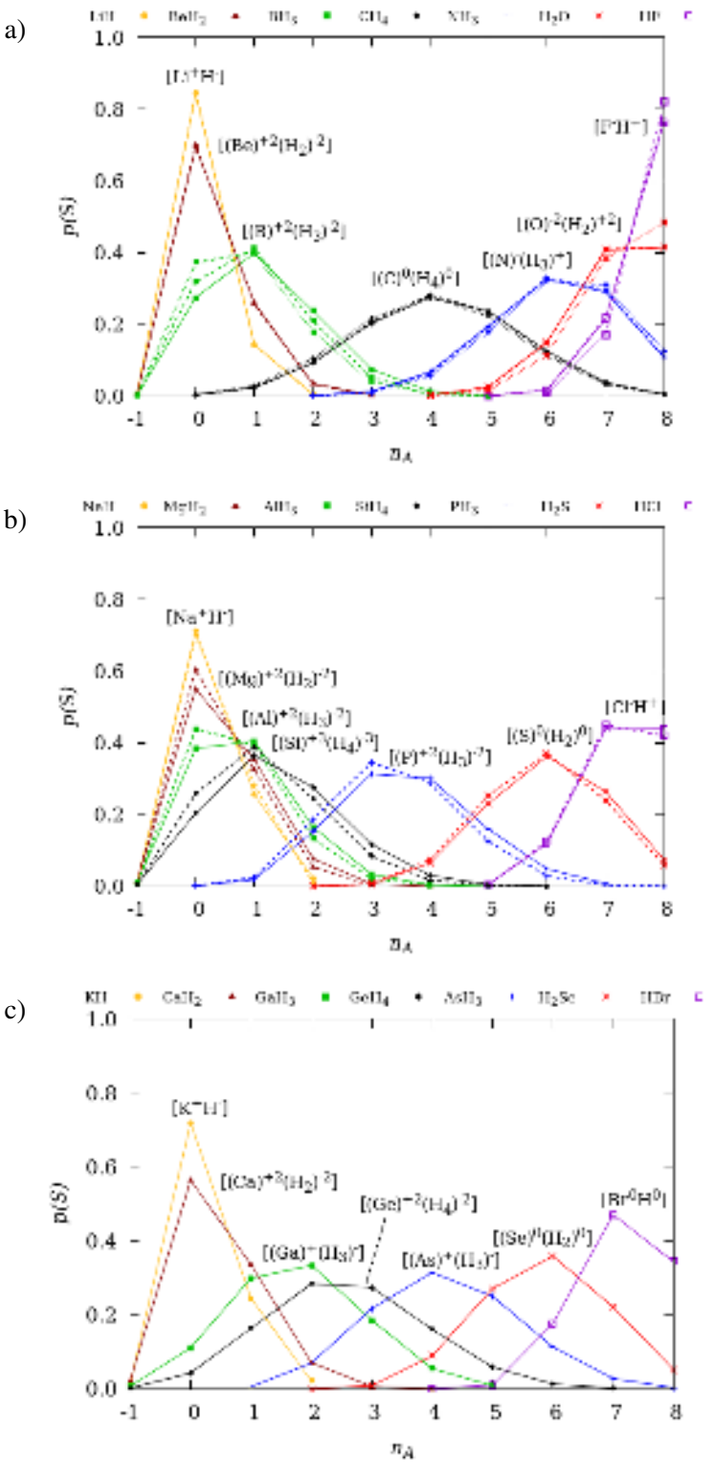

FIG. 2. 2-basin probabilities in the QTAIM framework for a) second-row, b) third-row, and c) fourth-row AH_n hydrides. B3LYP results are indicated in solid lines; CASSCF results are represented using dashed lines for a) and b); HF results are only displayed for a) using dotted lines. The most probable RSRS with B3LYP wave functions is given for each system. The meaning of n_A is explained in the text.

latter dominated by a single RSRS (with a probability of 0.768) assigning the 10 electrons to F (the neutral RSRS has a probability of 0.215). Note that the absence of a core in the hydrogen atom forbids $n_A > 8$ in HF, making this system more covalent than it would otherwise be.

We now turn our attention to the analysis of how chemical bonding evolves as we change the period (see Figure 2a-c). In this regard, we can see that alkali-based systems retain a common predominant ionic character, as evidenced by the $[A^+H^-]$ RSRS being dominant. Nevertheless, the probability of the distribution widens as we move from Li to Na and K compounds, and at the same time the probability of the main (ionic) RSRS decreases from 0.843 for LiH to 0.711 and 0.719 for NaH and KH, respectively, in favor of $[A^0H^0]$ (from 0.145 for LiH to 0.256 for NaH and 0.245 for KH). Thus, despite the higher electronegativity of Li –which, considering that H is more electronegative than Li, Na, and K, leads to the lowest electronegativity difference in LiH–, LiH would be the most ionic system. These results also reveal the different chemical behavior of the head element in a given group. Similar conclusions can be drawn for the alkaline earth hydrides. The tetrel group (14) deserves a special comment. As already explained, CH_4 is characterized by a broad distribution with a peak at $[C^0(H_4)^0]$, indicating a high covalent character. The picture changes significantly for SiH_4, whose EDF profile is significantly shifted to the right, as represented by the most probable RSRS being $[Si^{3+}(H_4)^{3-}]$ (0.364), in line with the well-known differences between C- and Si-based bonds. Interestingly, this trend is partially reversed in the case of GeH_4, for which the RSRS peak shifts to $[Ge^{2+}(H_4)^{2-}]$ (0.284), whose probability is almost equal to that of $[Ge^+(H_4)^-]$ (0.274). Such observations reveal, even more clearly than in the previous cases, (i) the chemical distinctiveness of the head element of the group, which shows an increased electronegativity, and (ii) how, in the third row, the effective electronegativity increases again. That is, (among the examples considered) C is the most electronegative element of the tetrel family ($\chi = 2.55$ on the Pauling scale), followed by Ge ($\chi = 2.01$) and Si ($\chi = 1.90$); then, when bonded to hydrogen ($\chi = 2.2$), the covalent character will follow the sequence C-H > Ge-H > Si-H, as revealed by the EDF analysis. Broadly speaking, the same conclusions could be drawn by examining the pnictogen (15), chalcogen (16), and halogen (17) groups.

In general, the observed trends correspond to the widely used rule of similarity across left diagonals between the 2^{nd} and 3^{rd} row p-block elements. These are the cases of the BH_3 and SiH_4, NH_3 and H_2S, or H_2O and HCl pairs. It has traditionally been explained by experimental properties such as differences in ionization potentials and ionic radii, and later by electronegativity similarities.[55] Focusing on a representative case, the BH_3 - SiH_4 couple shows a very similar RSRS

probability of 0.398 (BH_3) and 0.364 (SiH_4) at the EDF peak, with 5 relevant RSRS and a similar probability distribution. Similarly, CASSCF calculations increase the probability of n_A=0 for both cases compared to B3LYP (0.319 for BH_3, 0.258 for SiH_4) without changing the position of the maximum, at the expense of a decrease in the lower right tail probabilities. Overall, this results in similar chemical behavior, guided by analogous electronic distributions, despite different central element partial charges.

The effect of electron correlation has been evaluated by comparing Hartree-Fock, CAS and DFT (B3LYP) results. The results show that, in general terms, B3LYP provides an acceptable description of the systems under study. We refer the reader to the Supporting Information for a more insightful analysis of such effects.

To attain a finer partition of the chemical space in the framework of the QTAIM, we examine now group 14 (Table I). The results of all the other hydride systems within a multi-basin partition are provided in the Supporting Information (see Tables S10-S14), where interested readers can also find a detailed description of the results concerning group 15. This approach allows us to dissect the distributions described earlier into more detailed ones. Note that the ensuing discussion is focused on B3LYP results, the findings from CASSCF calculations for some selected systems being provided in the Supporting Information.

For CH_4, the neutral RSRS (i.e., the one in which the number of electrons of each atom corresponds to the number of electrons in the isolated atom) is the most relevant one (0.056), as shown in Table I. Nonetheless, the distributions in which an additional electron is transferred from H to C, or vice versa, are also relevant, with probabilities of 0.032 and 0.026, respectively. Moreover, when considering the sum of the several degenerate distributions (four in both cases), the accumulated probabilities (0.123 and 0.112, respectively) are higher than that of the main RSRS. The similar weights of the aforementioned distributions bring us back to the pattern extracted from Fig. 2a for CH_4, where a highly symmetric distribution predominates as a consequence of the high covalent character of C-H bonds. In line with this result, the following three RSRSs, listed in order of relevance (with relatively comparable weights), correspond to distributions where two C atoms accumulate 6 electrons (two more than in the neutral atom) at the expense of the population of two H basins (0.018), those where an electron is transferred from an H basin to an equivalent one while maintaining 4 electrons in C (0.015), or those in which two electrons are transferred from a C atom (that bears 2 electrons) to two different H basins (0.011). The distinctly different chemical bonding in SiH_4 as compared to that in CH_4 can be inferred at first glance from the EDF

TABLE I. Multi-basin EDFs for the QTAIM partition of group 14 hydrides. Only the most relevant distributions (above a threshold of 0.010) at the B3LYP level of theory are shown. Averaged probabilities are given in the case of equivalent-by-symmetry basins whose degeneracy is given by the multiplicity value.

System	$p(S)$	Mult.	n_{A}	n_{H1}	n_{H2}	n_{H3}	n_{H4}
CH_4	0.056	1	4	1	1	1	1
	0.032	4	5	0	1	1	1
	0.026	4	3	1	1	1	2
	0.018	6	6	0	0	1	1
	0.015	12	4	0	1	1	2
	0.011	6	2	1	1	2	2
SiH_4	0.129	1	0	2	2	2	2
	0.069	4	1	1	2	2	2
	0.033	6	2	1	1	2	2
	0.015	4	3	1	1	1	2
GeH_4	0.036	6	2	1	1	2	2
	0.036	4	3	1	1	1	2
	0.033	1	4	1	1	1	1
	0.033	4	1	1	2	2	2
	0.028	1	0	2	2	2	2
	0.010	4	2	0	2	2	2
	0.010	12	3	0	1	2	2

results. The most relevant RSRS for CH_4 does not even appear in Table I for SiH_4, as it displays a probability of 0.006. In contrast, the most significant RSRS corresponds now to a configuration in which Si atoms lack any valence electrons (note that core electrons, not included in Table I, are retained), and each H domain accommodates 2 electrons (0.129). The subsequent RSRSs in terms of relevance involve successive transfers of 1 (0.069), 2 (0.033), or 3 (0.015) electrons from a H basin in the main RSRS to Si. In the case of GeH_4, an intermediate behavior in terms of bond covalency is revealed. Unlike previous cases, the distribution is not predominantly governed by a single RSRS. Instead, a more *democratic* representation emerges, with five distributions carrying probabilities ranging from 0.028 to 0.036. Notably, the main RSRSs of CH_4 and SiH_4 are en-

compassed within this range, with probabilities of 0.033 and 0.028, respectively. Due to the ionic character of the molecule (although lower than for SiH_4), other distributions involve scenarios where Ge atoms bear fewer valence electrons than the neutral atom.

B. EDFs on ELF basins

As mentioned above, probably the greatest strength of the ELF partition is its ability to reconstruct the Lewis picture of molecular systems. ELF basins are typically classified according to their synaptic order (the number of core regions they are in contact with), a concept that can be related to the type of Lewis entity a given basin represents. In particular, the systems considered in this section show three types of ELF basins: cores, C(A), and lone pairs, V(A), which are monosynaptic; and disynaptic hydrogen (or hydrogenic), V(H,A), basins, associated with the A-H bonds.

First, we used two flavors of the 2-region EDF analysis, namely: (i) the C(A) basin and $\mathbb{R}^3$-C(A), and (ii) one of the equivalent V(A,H) basins together with the remaining space, $\mathbb{R}^3$-V(A,H) (provided in the Supporting Information, Table S18-S19). Our results are in agreement with previous studies performed by other authors,[56] and, since ELF 2-region probabilities have been regularly published using the above-mentioned recursion algorithm[14] and the results are not especially intuitive from a chemical point of view, we will start directly with a multi-basin analysis. Note that we have used the same notation for electron counting as for QTAIM (and QEI) basins. As a result, only *n*s and *n*p valence electrons are reported, with the reference (neutral) population of cores being established at zero. This means that a formal population of zero in the cores of 2^{nd}-row systems accounts for 2 electrons, in 3^{rd}-row systems for 10, and in 4^{th}-row systems for 18. The emergence of several negative populations in the core (vide infra) simply points out situations where the core regions harbor fewer electrons than the sum corresponding to fully occupied shells in the traditional neutral atom's core, that is, lower than 2, 10 and 18 for 2^{nd}-, 3^{rd}- and 4^{th}-row atoms, respectively.

Systems from groups 14 to 16 were analyzed using a 5-basin spatial division covering all ELF basins, while in group 17 all the degenerate V(A) basins were combined, leaving only three domains (data for the remaining groups is provided in SI, Table S20-S26). In all cases, the classical Lewis distribution picture (i.e. the one that assigns two electrons to each covalent bond or lone pair) is found to be the most relevant one, except in the HF molecule, where the lone pair region

TABLE II. Multi-basin EDFs for the ELF partitioning in the saturated AH_n hydrides of elements of groups 14 and 15, for the 2^{nd}, 3^{rd} and 4^{th} rows (results at the B3LYP level). Only the most relevant distributions are shown: above a threshold of 0.005 for group 14 and 0.015 for group 15 (set for 2^{nd} row hydrides); additional information is provided in Tables S22 and S23. Averaged probabilities are given in the case of equivalent-by-symmetry basins whose degeneracy is given by the multiplicity value.

						$p(S)$		
$n_{C(A)}$	$n_{V(H1,A)}$	$n_{V(H2,A)}$	$n_{V(H3,A)}$	$n_{V(H4,A)}$	Mult.	CH_4	SiH_4	GeH_4
0	2	2	2	2	1	0.192	0.303	0.142
0	1	2	2	3	12	0.034	0.026	0.017
1	1	2	2	2	4	0.017	0.025	0.024
0	1	1	3	3	6	0.008	0.004	0.003
-1	2	2	2	3	4	0.007	0.019	0.035
$n_{C(A)}$	$n_{V(H1,A)}$	$n_{V(H2,A)}$	$n_{V(H3,A)}$	$n_{V(A)}$	Mult.	NH_3	PH_3	AsH_3
0	2	2	2	2	1	0.116	0.163	0.090
0	1	2	2	3	3	0.042	0.037	0.026
0	2	2	3	1	3	0.030	0.029	0.018
0	1	2	3	2	6	0.028	0.024	0.015
1	2	2	2	1	1	0.015	0.024	0.026

carries an extra electron extracted from the H-F bond[57–59]. We now focus on the tetrel representatives, for which the classical Lewis representation (two electrons in each bond) is dominant in all three cases (Table II top): its probability goes from 0.192 for CH_4 to 0.303 for SiH_4 and 0.142 for GeH_4, in agreement with the QTAIM results. Other distributions also show significant changes, such as the scenario where an electron is transferred from one V(H,A) basin to another, with probabilities decreasing from 0.034 for CH_4 to 0.026 for SiH_4 and 0.017 for GeH_4. Conversely, the likelihood of distributions in which an electron is transferred from an A-H basin to the core is larger for SiH_4 and GeH_4 (0.025 and 0.024, respectively) than for CH_4 (0.017). In a similar way, the opposite phenomenon exhibits a significant increase in probability from CH_4 (0.007) to SiH_4 (0.019) and to GeH_4 (0.035), which can be explained by the increase in volume of the core basin from C to Ge.

The preceding analysis shares many similarities with what is found in the pnictogens. The

distinguishing factor here is the presence of a lone pair basin, which is absent in group 14 systems. The most likely structure is the classical Lewis EDF with two electrons in each bond and the lone pair, with probabilities following the order: PH_3 (0.163) > NH_3 (0.116) > AsH_3 (0.090). This, again, points to the distinctive character of phosphine. In all cases, the next most probable distribution involves an electron transfer from an A-H basin (accommodating one electron) to the lone pair (with an occupancy of three), with this possibility being more favored for NH_3. The transfer of an electron from a valence basin to the A core is much more likely in the 3^{rd} and 4^{th} row systems, which have larger cores. In agreement with chemical intuition, this transfer involves the lone pair. Roughly analogous results are obtained in the systems of the chalcogen and halogen groups and are therefore not discussed further.

Overall, while the EDF bonding picture in terms of the ELF might be less intuitive than that obtained in terms of QTAIM basins, it illustrates the main concepts of bond polarity and ionicity/covalency in terms of the well-established and intuitive chemical language based on Lewis entities.

C. EDFs on ELF∩QTAIM intersections

As we have tried to show, the EDFs of the QTAIM and ELF partitions provide a wealth of information about the electron distribution in molecules that is necessarily framed within the atomic and Lewis descriptions, respectively. By appealing to the finer decomposition of ELF∩QTAIM (QEI), we expect to get the best of the two worlds and analyze the bonding picture simultaneously in terms of both, atom- and Lewis-based pictures. With this approach, we decompose polysynaptic ELF basins (those representing covalent bonds between multiple atoms) into contributions arising from the number of core atoms they connect (i.e., the synaptic order) while leaving core and lone pair domains unchanged (as they belong to the same QTAIM basin). All bonding regimes considered in this section contain disynaptic ELF basins, which are thus split into two new domains. Since we are considering A-H bonds, the V(H,A) basins are divided into two contributions: the one corresponding to $\Omega_A \cap$ V(H,A), giving rise to the bond subregion $B^A_{H\text{-}A}$, and another resulting from the intersection of $\Omega_H \cap$ V(H,A), which will be referred to as $B^H_{H\text{-}A}$. Given the peculiarities of hydrogenic ELF basins, the latter is the diffuse hydrogen-exclusive sub-region but does not properly correspond to a C(H) core region (see Fig. 3). In line with the previous discussion, the presented results correspond to B3LYP, unless otherwise stated.

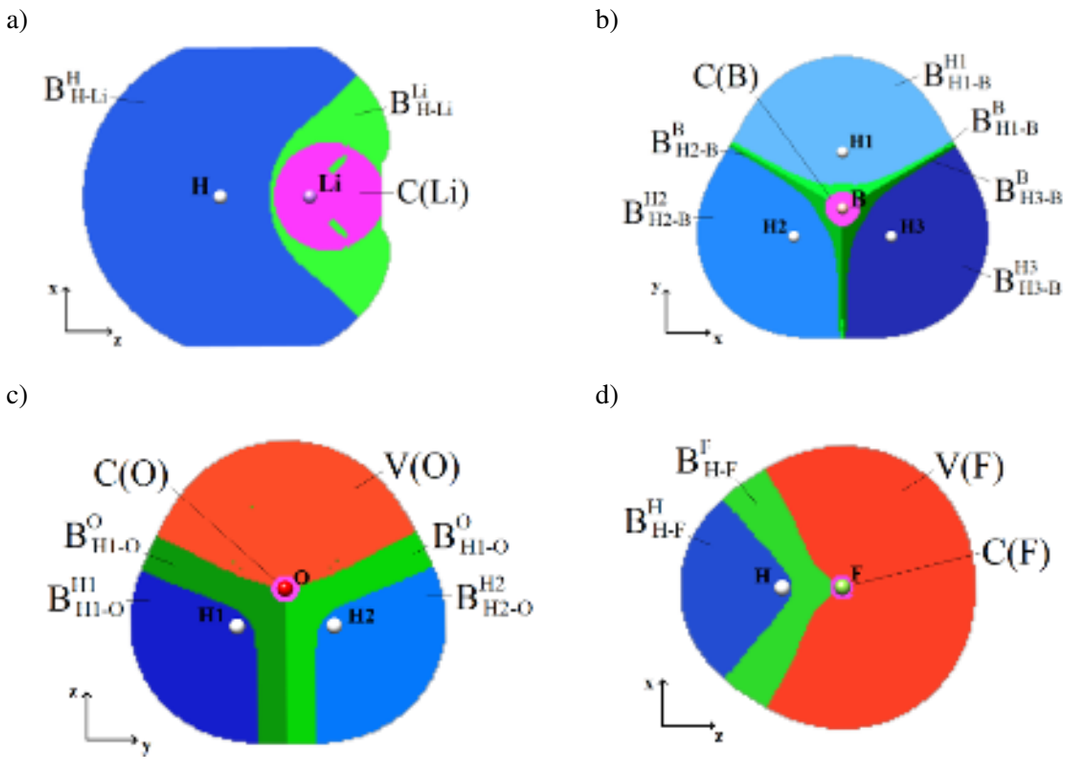

FIG. 3. ELF∩QTAIM partitioning for a) LiH, b) BH_3, c) H_2O, d) HF projected on the σ_h plane. Bluish: hydrogen sub-region, $B^{H}_{H\text{-}A}$; greenish: disynaptic bond sub-region, $B^{A}_{H\text{-}A}$; pink: central atom core sub-region, C(A); orange: monosynaptic V(A) region. Note that different basins of the same type in the same molecule are coloured by suing different color tones.

We initially analyzed the two 2-basin EDF distributions that arise when considering the topological partition of space involving either the $B^{A}_{H\text{-}A}$ or $B^{H}_{H\text{-}A}$ domain and the rest of the molecule (Figure 4, extended data being provided in Tables S27 and S29). Consistent with previous findings, 2nd-row hydrides exhibit three distinct tendencies. When inspecting the EDF analysis based on $B^{H}_{H\text{-}A}$ and $\mathbb{R}^3$-$B^{H}_{H\text{-}A}$ basins (Figure 4 top left), one can see that the most ionic systems where the A atom carries a partial positive charge (LiH and BeH_2), showcase a probability peak at $n_{B^{H}_{H\text{-}A}} = 2$, with minimal variations between B3LYP (0.843 LiH, 0.798 BeH_2) and CAS (0.848 LiH, 0.795 BeH_2) results. In other words, the hypothetical two electrons corresponding to a *"pure"* single A-H bond are located in the H region. The second most probable distribution is characterized by a population of one in the $B^{H}_{H\text{-}A}$ basin, though the probabilities are significantly lower (0.145 LiH, 0.170 BeH_2, both B3LYP), aligning with the high ionic character of the bond.

Nonetheless, distinctions between both systems highlight the higher ionicity of LiH. A con-

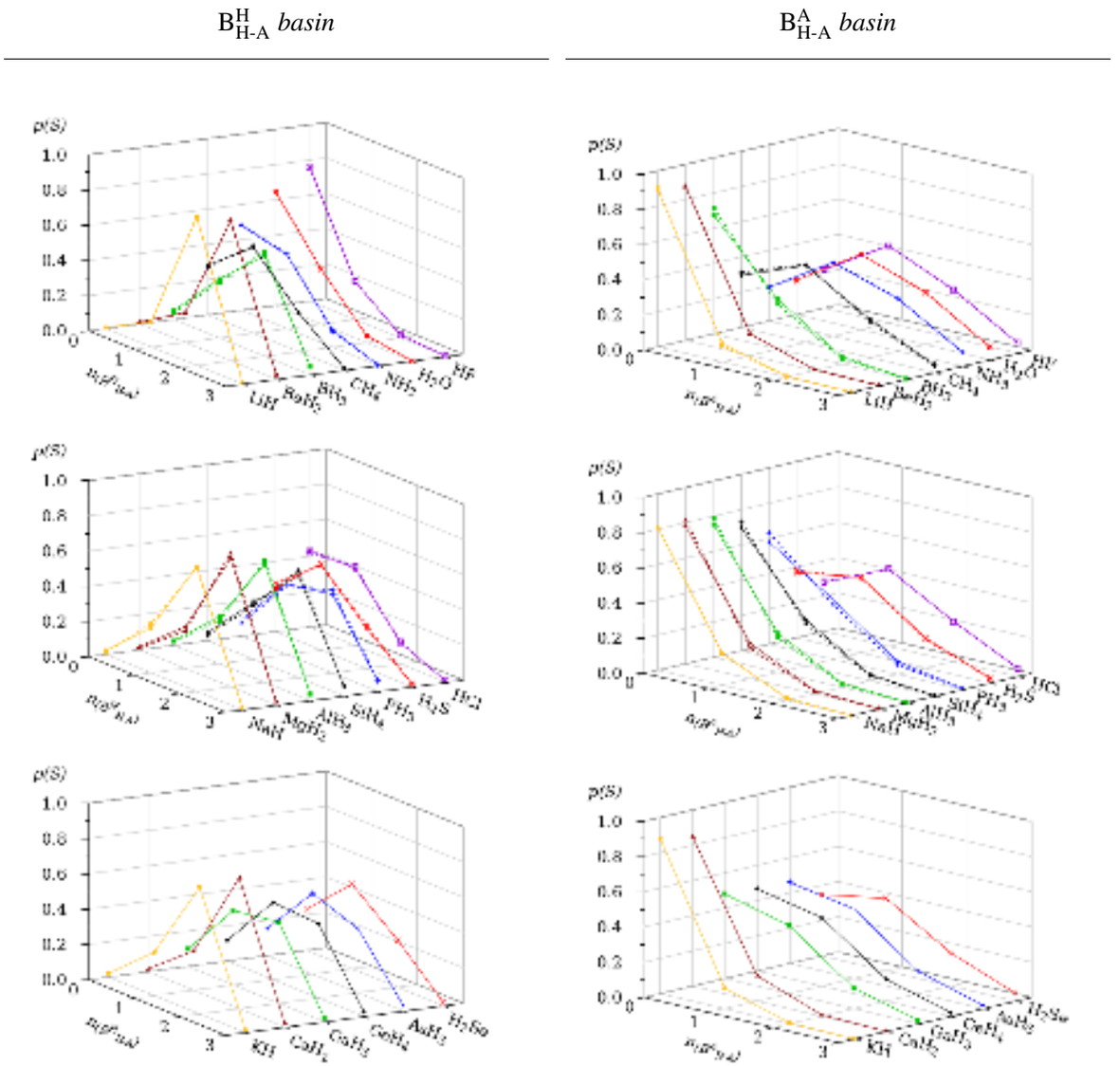

FIG. 4. 2- basin probabilities for hydrogen ($B^{H}_{H\text{-}A}$)(left) and bond ($B^{A}_{H\text{-}A}$) (right) sub-regions within QEI partition in second-row (top), third-row (middle) and fourth-row (bottom) AH_n hydrides. Solid lines: B3LYP wave function; dashed lines: CASSCF calculations.

sistent behavior is observed when analyzing the 2-basin EDF based on $B^{A}_{H\text{-}A}$ and $\mathbb{R}^3$-$B^{A}_{H\text{-}A}$ basins (Figure 4 top right). In this case, the distribution is predominantly dominated by a peak corresponding to $n_{B^{A}_{H\text{-}A}} = 0$ (0.892 LiH, 0.873 BeH_2), followed by that with $n_{B^{A}_{H\text{-}A}} = 1$ (0.105 LiH, 0.122 BeH_2). The increase in electronegativity of B (w.r.t. Li and Be) is reflected in BH_3, characterized by a decrease in the probability of the $n_{B^{H}_{H\text{-}B}} = 2$ peak (0.572), accompanied by a higher weight of $n_{B^{H}_{H\text{-}B}} = 1$ (0.333).

A distinct response emerges at the turning point represented by CH_4, for which the probability peak of $B^{H}_{H\text{-}C}$-based EDFs shifts to $n = 1$ (0.486). The probabilities of $n_{B^{H}_{H\text{-}C}} = 0$ and $n_{B^{H}_{H\text{-}C}} = 2$ become relatively similar (0.281 and 0.222, respectively), aligning with its highly covalent character. This pattern remains consistent when examining $B^{C}_{H\text{-}C}$ EDFs, where $p(n_{B^{C}_{H\text{-}C}} = 1) = 0.438$. The probabilities of empty and double-populated $B^{C}_{H\text{-}C}$ structures are 0.303 and 0.213, respectively.

The third group includes systems with bonds polarized toward the A atom, specifically NH_3, H_2O, and HF. The most probable distribution in the $B^{H}_{H\text{-}A}$-based analysis is the one where this basin is empty (probabilities equal to 0.481, 0.645, and 0.769, respectively), followed by the configuration where it accommodates one electron (0.417, 0.313, and 0.215, respectively). It is noteworthy that this behavior is consistent with the chemical expectations when considering the increasing electronegativity of the A atom: as it rises, the $B^{H}_{H\text{-}A}$ basin becomes depopulated due to the electron being polarized toward A, which explains why HF has the highest weight for the structure with $n_{B^{H}_{H\text{-}A}} = 0$.

The $B^{A}_{H\text{-}A}$-based EDFs in this group show a peak located at $n_{B^{A}_{H\text{-}A}} = 1$ (instead of 2), with values quite similar in all systems: 0.421 for NH_3, 0.428 for H_2O, and 0.439 for HF. The next structure in relevance is the one that accumulates both bonding electrons at the A center, $n_{B^{A}_{H\text{-}A}} = 2$, again with very similar weights (0.294 for NH_3, 0.296 for H_2O, and 0.278 for HF). Note that, taken together, these QEI probabilities exhibit either an exponentially decreasing or a parabolic dependence on n.

Provided that only if $p(S)$ for a given basin has a maximum can we say that the basin effectively harbors electrons (for only in this case does it act as an electronic buffer), we can binarily classify the QEI subregions as empty or filled. Indeed, if the two sub-regions are filled, they can be said to host one electron each, while if one of them is empty, the other accumulates both electrons of the pair. This binary classification thus assigns one or two of the electrons of a pair to each of the centers of the disynaptic basin, and following the reasoning exploited with great success by the groups of Head-Gordon first,[60] and Salvador later,[61] it can be used to introduce formal oxidation states. This is a very relevant result that we expect to exploit shortly. With this classification, for instance, methane is covalent while silane is ionic.

When we turn to the third and fourth row hydrides, significant differences become apparent. Focusing first on groups 1, 2, and 13 (highly ionic systems with the A center positively charged), the probability that the A-H bond electrons are at the A center decreases. In other words, there is an increase in the $B^{H}_{H\text{-}A}$ probabilities and a decrease in the $B^{A}_{H\text{-}A}$ ones (see the yellow, brown, and green lines in Figure 4). The variations in the alkali and alkaline earth groups when moving to the

fourth row are noticeable but smooth, while the boron group presents a much abrupt change. In any case, the EDF profiles shift to situations in which the A atom acquires more relevance in the bonding. Namely, in GaH_3, the probability of $n_{B^{A}_{H\text{-}A}} = 1$ increases from 0.219 in AlH_3 to 0.382 in GaH_3, at the expense of $n_{B^{A}_{H\text{-}A}} = 0$ (0.759 and 0.485, respectively). The same conclusions can be drawn when analyzing $B^{H}_{H\text{-}A}$-based EDFs. From groups 14 to 17, we observe a pronounced decrease in the probability of bonding electrons being assigned to the A center when moving from second to third-row systems. This is especially evident when analyzing $B^{A}_{H\text{-}A}$-based EDFs, which show that, for example, the probability of such basin accumulating 0 electrons increases from 0.296 to 0.695 in the cases of CH_4 and SiH_4.

Note that $n_{B^{H}_{H\text{-}A}}$ becomes more homogeneous as we go down from the 2^{nd} to the 4^{th} row. Indeed, in the fourth row all $n_{B^{H}_{H\text{-}A}}$ show a local maximum. A similar behavior is observed in $n_{B^{A}_{H\text{-}A}}$. This is a consequence of lower and similar electronegativities for the central atoms in this series.

A multi-basin EDF analysis is now performed by taking several EQI basins. Depending on the system, the number of EQI subregions varies from three in the Group 1 hydrides - C(Li), $B^{H}_{H\text{-}Li}$ and $B^{Li}_{H\text{-}Li}$ - to an almost unmanageable number in group 14 systems - C(C) and eight additional basins derived from the partition of the four C-H bonds. To facilitate the analysis, the systems have been divided into three different categories: (i) alkali hydrides, for which a 3-basin EDF description is performed, (ii) groups 13, 14, and 17, for which we chose a 4-basin EDF analysis, and (iii) groups 2, 15, and 16, for which a 5-basin EDF is done (additional information is provided in Table S31-S37 from the Supporting Information).

Table III, top, gathers the results for the alkali hydrides. The dominant distribution is the Lewis one, with two electrons in the bond; nonetheless, the QEI analysis unveils how the two electrons are preferentially hosted in the H "part" of the bond, that is, in the $B^{H}_{H\text{-}A}$ basin, a situation that can be referred to as an *ionic* Lewis structure. As expected, the probability of this dominant distribution decreases from LiH (0.815) to NaH (0.678), while it shoots up slightly in KH (0.690). Note that the depopulation of the previous structure in NaH is mainly due to electron transfer from the hydride to the Na part of the bond basin (0.134), a covalent-like structure (with one electron in $B^{H}_{H\text{-}A}$ and the other in $B^{A}_{H\text{-}A}$), while in KH the distribution in which the electron is transferred to the K core acquires more relevance (0.164), which is likely related to the availability of low-lying d-states in K that are absent in Na (0.117). Overall, the aforementioned covalent-like distribution increases in importance from LiH (0.074) to NaH (0.134), while it decreases again for KH (0.078).

The complete space analysis via 5-basin EDFs is offered in the alkaline-earth moieties (Table

TABLE III. QEI multi-basin EDF probabilities for groups 1 and 2 AH_n species calculated at the B3LYP level. Only the most relevant distributions are shown (above a threshold of 0.010). As in previous Tables, symmetry is considered, and averaged values are provided when applicable.

				$p(S)$		
$n_{C(A)}$	$n_{B^A_{H\text{-}A}}$	$n_{B^H_{H\text{-}A}}$	Mult.	LiH	NaH	KH
0	0	2	1	0.815	0.678	0.690
0	1	1	1	0.074	0.134	0.078
1	0	1	1	0.069	0.117	0.164
-1	1	2	1	0.027	0.033	0.029

$n_{C(A)}$	$n_{B^A_{H1\text{-}A}}$	$n_{B^A_{H2\text{-}A}}$	$n_{B^{H1}_{H1\text{-}A}}$	$n_{B^{H2}_{H1\text{-}A}}$	Mult.	BeH_2	MgH_2	CaH_2
0	0	0	2	2	1	0.631	0.476	0.497
0	0	1	2	1	2	0.067	0.093	0.068
1	0	0	2	1	2	0.041	0.049	0.084
0	1	0	2	1	2	0.017	0.020	0.008
0	0	0	3	1	2	0.017	0.006	0.005
-1	1	0	2	2	2	0.014	0.027	0.025

III, bottom). As expected, the *ionic* Lewis structure (two electrons in each bond, but both assigned to the hydrogen domain) dominates in the three cases, although its probability is considerably higher in BeH_2 (0.631) than in the other two systems. Interestingly, this ionic distribution has minimal probability in MgH_2 (0.476), rising again in CaH_2 (0.497). This behavior is very similar to that found in the alkali hydrides, and again points to the effect of available d-states in Ca. A closer inspection reveals that in both the beryllium and the magnesium hydrides the next most probable structure is a more covalent one in which an electron is transferred from the H-domain of one of the A-H bonds to the A counterpart (probabilities of 0.067 and 0.093, respectively). However, in line with KH, in CaH_2 the electron is preferentially transferred to the Ca core (0.084 *vs* 0.068). Taken together, these data support a non-negligible role of d electrons in heavy alkaline and alkaline-earch hydrides. Note that the geometrical structure of CaH_2 is not linear and that d-orbital participation, which is quite clear in NBO descriptions, has been invoked to understand this behavior.[62]

TABLE IV. 4-QEI basin EDF probabilities for the hydrides of groups 13 and 14 AH_n, all calculated at the B3LYP level. Only the most relevant distributions are shown for each hydride (above a threshold of 0.020 for group 13 and 0.025 for group 14, with respect to the 2^{nd} row hydrides). Results have been averaged for all the equivalent-by-symmetry A-H bonds present in the molecules.

				$p(S)$		
$n_{C(A)}$	$n_{B^A_{H\text{-}A}}$	$n_{B^H_{H\text{-}A}}$	$\cup(AH_2)$	BH_3	AlH_3	GaH_3
0	0	2	4	0.420	0.464	0.173
0	1	1	4	0.142	0.100	0.114
0	0	1	5	0.095	0.060	0.047
0	1	2	3	0.057	0.036	0.035
1	0	2	3	0.049	0.074	0.055
1	0	1	4	0.039	0.049	0.047
0	0	3	3	0.035	0.024	0.006
-1	0	2	5	0.021	0.052	0.076
$n_{C(A)}$	$n_{B^A_{H\text{-}A}}$	$n_{B^H_{H\text{-}A}}$	$\cup(AH_3)$	CH_4	SiH_4	GeH_4
0	1	1	6	0.211	0.103	0.101
0	0	2	6	0.119	0.352	0.137
0	2	0	6	0.092	0.007	0.018
0	0	1	7	0.085	0.087	0.054
0	1	0	7	0.071	0.012	0.019
0	2	1	5	0.064	0.010	0.020
0	1	2	5	0.049	0.049	0.037
1	1	1	5	0.039	0.023	0.037
1	0	1	6	0.027	0.045	0.040

The 4-basin EDF results for groups 13 and 14 are shown in Table IV. The following regions were considered: $B^H_{H\text{-}A}$, $B^A_{H\text{-}A}$ (both arising from the same V(A,H) basin), C(A), and the remaining fragment of the molecule. The most likely distribution in group 13 is the one with the two bonding electrons in the $B^H_{H\text{-}A}$ basin and the remaining four valence electrons in the additional fragment representing the "rest of the molecule" (i.e. the other two A-H bonds), compatible with an ionic

description and with probabilities equal to 0.420 and 0.464 for BH_3 and AlH_3, respectively. Notice that, in agreement with electronegativity arguments, the ionic structure peaks at AlH_3. Interestingly, the probability of this RSRS drops sharply for GaH_3 (0.173), which has many other low probability distributions not shown. Note that since the core contains 3d electrons in this case, it easily harbors more electrons, and that the higher entropy of the EDF points to a distinctive bonding situation that will also be found in other cases below. The significance and possible relation of this behavior to the higher metallic character of the bond to the central atom remains to be investigated.

Group 14 hydrides show two different behaviors. In CH_4, as expected, the most likely distribution is the pure covalent-like (0.211), which assigns two electrons to each A-H bond, and, out of the two electrons hosted in the V(A,H) basin under study, 1 electron is assigned to each atomic domain ($B^{H}_{H\text{-}A}$ and $B^{A}_{H\text{-}A}$). The next RSRS also corresponds to a Lewis one (two electrons in each V(C,H) basin), but in which both electrons are hosted in the $B^{H}_{H\text{-}A}$ basin (0.119), closely followed by the symmetric alternative, that is, hosting both electrons in the $B^{A}_{H\text{-}A}$ basin (0.092). In both silane and germanane, the most likely distribution is the *ionic* Lewis one in which both electrons of the V(A,H) basin are associated to the A atomic region ($B^{A}_{H\text{-}A}$ basin), with probabilities of 0.352 and 0.137, respectively. This difference carries over to the rest of the distributions shown in the table, where SiH_4 and GeH_4, but not CH_4, tend to minimize structures populating the $B^{A}_{H\text{-}A}$ basin.

As previously stated, from group 15 on a limited number of basins, never exceeding five, is considered in the discussion to allow for a comprehensible analysis (see Table V). These are, in addition to the core, one lone pair, V(A), the two basins ($B^{H}_{H\text{-}A}$ and $B^{A}_{H\text{-}A}$) that result from splitting a given A-H bond, and the basin that represents the "rest of the molecule".

In ammonia the most probable distribution (0.081) corresponds to the covalent Lewis-like one, with one electron in each $B_{H\text{-}A}$ basin, with the distribution in which both V(A,H) electrons lie in the A side ($n_{B^{A}_{H\text{-}A}} = 2$) being close (0.070). The main distribution domain for NH_3 is ranked second in PH_3 and AsH_3 (0.067 and 0.050, respectively), in favour of the distribution in which both V(A,H) electrons are accommodated in the $B^{A}_{H\text{-}A}$ basin (0.134 and 0.060, respectively). Such difference is quite indicative of the different bonding regimes in the three systems, intuitively revealing that the covalent character decreases sharply from to NH_3 to PH_3 and then increases smoothly for AsH_3. Other relevant distributions for PH_3 and AsH_3 also involve depopulation of the $B^{A}_{H\text{-}A}$ basin, in agreement with the previous discussion.

The comparison of NH_3 with CH_4 and H_2O is also quite illustrative. The latter exhibits a main

TABLE V. Multi-basin QEI EDF probabilities in the saturated hydrides of groups 15 and 16 from B3LYP results. Only the most relevant distributions are shown (above a threshold of 0.040 for at least one distribution). Results have been averaged for all the equivalent-by-symmetry A-H bonds present in the molecules.

					$p(S)$		
$n_{C(A)}$	$n_{V(A)}$	$n_{B^A_{H\text{-}A}}$	$n_{B^H_{H\text{-}A}}$	$\cup(AH_2)$	NH_3	PH_3	AsH_3
0	2	1	1	4	0.081	0.067	0.050
0	2	2	0	4	0.070	0.008	0.010
0	3	1	0	4	0.043	0.010	0.010
0	2	1	0	5	0.042	0.010	0.009
0	3	1	1	3	0.042	0.027	0.024
0	3	0	1	4	0.025	0.042	0.027
0	2	0	1	5	0.025	0.042	0.023
0	2	0	2	4	0.023	0.134	0.060
0	3	0	2	3	0.011	0.048	0.026
$n_{C(A)}$	$n_{V(A)}$	$n_{B^A_{H\text{-}A}}$	$n_{B^H_{H\text{-}A}}$	$\cup(AH)$	H_2O	H_2S	H_2Se
0	2	2	0	4	0.076	0.027	0.013
0	2	1	0	5	0.062	0.027	0.014
0	3	1	0	4	0.062	0.024	0.012
0	2	1	1	4	0.053	0.075	0.042
0	3	2	0	3	0.047	0.014	0.007
0	2	0	2	4	0.009	0.050	0.033

RSRS (0.076) in with two valence electrons are assigned to the considered lone pair, two to the $B^A_{H\text{-}A}$ basin, and the remaining four to the "rest of the molecule". That is, the two electrons of the V(H,A) basin lie preferentially in the O domain. The two following RSRSs can be described as an electron transfer from the $B^A_{H\text{-}A}$ basin in the previous structure to the "rest of the molecule", or to the lone pair of O atom (V(A) basin), both having a probability of 0.062. The fourth would correspond to the purely covalent one, in which the two electrons of the V(H,A) basin are equally assigned to $B^A_{H\text{-}A}$ and $B^H_{H\text{-}A}$ basins (0.053); which was the first in relevance in CH_4 and NH_3.

The QEI analysis also sheds light on the behaviour of HF molecule. When analysing ELF-

TABLE VI. Multi-basin QEI EDF probabilities in the saturated halogen hydrides from B3LYP results. Only the most relevant distributions are shown (above a threshold of 0.040 for at least one distribution).

				$p(S)$	
$n_{C(A)}$	$n_{V(A)}$	$n_{B^{A}_{H\text{-}A}}$	$n_{B^{H}_{H\text{-}A}}$	HF	HCl
0	7	1	0	0.218	0.105
0	6	2	0	0.172	0.093
0	8	0	0	0.083	0.035
0	6	1	1	0.074	0.136
1	6	1	0	0.073	0.040
0	7	0	1	0.049	0.079
1	5	2	0	0.046	0.028
0	6	0	2	0.008	0.047

based EDFs, we obtained a main distribution in which seven valence electrons are assigned to the lone pairs of F atom, and one remains in the V(H,A) basin (0.268, Table II), as expected by the extraordinarily high electronegativity of F. The QEI results reveal that there is a probability of 0.218 for the bonding electron lying in the $B^{A}_{H\text{-}A}$ region, and only 0.049 of it being in $B^{H}_{H\text{-}A}$ (see Table VI). Similarly, the total ELF based probability of the Lewis-like structure (six valence electrons in the lone pair and two in the H-F basin) is 0.255. The QEI partition allows to provide a finer understanding of such distribution, revealing that the probability of both bonding electrons being in $B^{A}_{H\text{-}A}$ is predominant (0.172), followed by that in which the two electrons are equally distributed in the $B^{A}_{H\text{-}A}$ and $B^{H}_{H\text{-}A}$ basins (0.074), while the probability of both electrons being simultaneously in the $B^{H}_{H\text{-}A}$ basin is residual (0.008). Similar trends (in terms of bonding nature) as those already provided in the previous discussion can also be extracted upon analyzing the variation of the RSRS probabilities along a given period in groups 15, 16, and 17 and are thus not repeated here (see Table V-VI).

D. Additional systems

After the previous comprehensive study of simple hydrides, we proceed to examine more intricate systems in an attempt to further delve into the potential of our approach to understand and

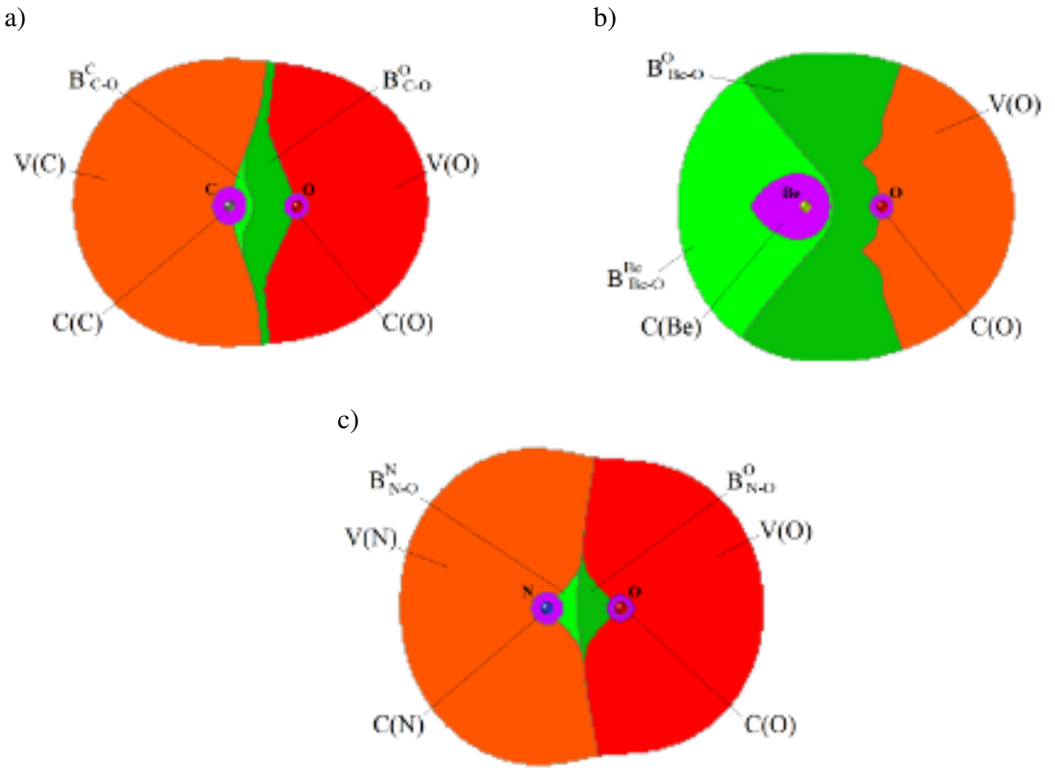

FIG. 5. QEI partitioning for a) CO, b) BeO and c) NO projected on a plane passing through the nuclei. Greenish: bond sub-regions, $B^{A}_{A\text{-}B}$; pink: core basins, C(A); orange: monosynaptic V(A) attractors. Note that different basins of the same type in the same molecule are colored with different color tones.

characterize chemical bonding. For such a purpose, various heterodiatomic oxides were studied: CO, BeO, and NO.

As for the former, the unique characteristics of its C–O bond have attracted the attention of numerous researchers who have approached the problem either from an orbital perspective or within the framework of quantum chemical topology.[63–65] For instance, employing the ELF partition, Silvi and coworkers were able to extract the probability of Lewis-like mesomeric structures as well as quantify the changes in the flexible electronic structure of the CO bond when, for instance, this species acts as a 1:1 ligand in metal complexes.[44,63,66,67]

The QTAIM EDF of a diatomic system provides more information than the strict average atomic population and its variance but is limited by its small number of non-negligible components. Fig. 6 (see the Supporting Information also) shows that, in the CO case, the distribution peaks at O^{-} and is considerably skewed toward oxygen due to the considerable electronegativity difference between the two atoms. On top of this overall electron transfer, we nevertheless observe

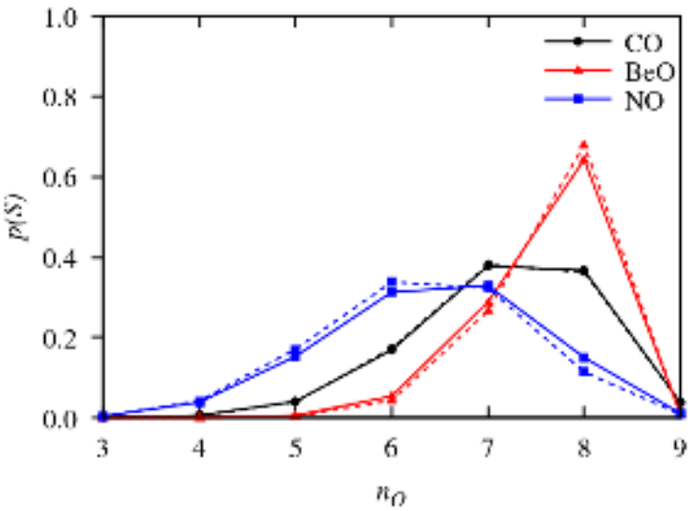

FIG. 6. EDF on QTAIM basins for the heterodiatomic CO (black), BeO (red) and NO (blue) molecules, at the DFT (solid lines) and CASSCF (dashed lines) levels, where the probability of each distribution is plotted as a function of the electron population in the oxygen basin (n_O), using the same counting notation used throughout the paper ($n_O = 8 \equiv O^{2-}$).

a considerable width that uncovers, as known, a large covalency.

Besides the two QTAIM atoms, the ELF partition displays five basins: the C(C) and C(O) core basins; the monosynaptic valence basins V(C) and V(O); and finally, the disynaptic valence basin V(C,O). Table VII gathers our results. Several interesting points emerge. The most relevant one is that, as is generally known from population averages,[63] the ELF bond basins in the case of nominally multiple bonds fall short of displaying the expected number of electron pairs. The peak probability in the present case is at 3 electrons ($p = 0.149$), with no single EDF component in the Table harboring 6 electrons within the C-O bond basin. The second relevant point regards the notable mobility of the bond electrons: we find several significant distributions with 1 to 5 electrons. Finally, the C and O lone pairs are also found to harbor a rather variable number of electrons. Although the largest probability distributions display more electrons in the oxygen than in the carbon lone pairs, it is not extremely unlikely to see the reverse situation. In other words, there is also considerable electron mobility between the C and O lone pairs mediated by the central bond basin. This could add to shed light on some very bitter disputes in the recent literature which we have already referred to, regarding the role of *outer* bonds in simple diatomics such as the C_2 molecule.[3,4]

TABLE VII. Three-basin ELF EDFs in the CO molecule at DFT level (above a threshold of 0.020). Core and monosynaptic basins (C(A) and V(A), being A a given atom) are merged in the same fragment for each atom.

$n_{\mathrm{C(C)\cup V(C)}}$	$n_{\mathrm{V(C,O)}}$	$n_{\mathrm{C(O)\cup V(O)}}$	$p(S)$
2	3	5	0.149
3	3	4	0.127
2	4	4	0.126
3	2	5	0.099
2	2	6	0.085
3	4	3	0.072
2	5	3	0.053
4	2	4	0.044
4	3	3	0.038
3	1	6	0.029
1	4	5	0.022

Moving to the QEI intersection, Table VIII shows very neatly how large the polarity of the CO molecule is. Most of the time, the $\mathrm{B}^{\mathrm{C}}_{\mathrm{C\text{-}O}}$ sub-region is empty, and the 3 electrons that the bond basin holds in the most probable arrangement lie in the $\mathrm{B}^{\mathrm{O}}_{\mathrm{C\text{-}O}}$ section. Notice also that, following the previous paragraph, the sub-basin associated with the O atom displays a much broader distribution than that of the carbon atom as a result of the lone pair mobility just discussed.

A thinner analysis is found in Table IX, where to the sub-regions of the CO bond valence basin we added two extra domains by grouping together all the other C and O domains, respectively. We think that these results show clearly that there is direct communication between the C and O monosynaptic domains, and that at least part of the electrons that are normally considered to engage in the CO π bonds are contained in the V(C) and V(O) ELF basins. By taking a quick look at the first rows of the Table one finds that delocalization takes place mainly either by electron transfer between the two lone pair domains, within the two parts of the CO bond valence, or between the O lone pair and the O sub-region of the CO bond valence, all as expected from the previous discussion. Notice also that almost 50% of all the probability is accounted for by distributions that harbor no electron in the $\mathrm{B}^{\mathrm{C}}_{\mathrm{C\text{-}O}}$ region.

TABLE VIII. Two-basin EDFs within the QEI framework considering the isolated $B^{C}_{C\text{-}O}$ (left) and $B^{O}_{C\text{-}O}$ (right) sub-regions. The results have been obtained at the DFT level of theory.

$n_{B^{C}_{C\text{-}O}}$	$n_{\mathbb{R}^3-B^{C}_{C\text{-}O}}$	$p(S)$	$n_{B^{O}_{C\text{-}O}}$	$n_{\mathbb{R}^3-B^{O}_{C\text{-}O}}$	$p(S)$
0	10	0.735	3	7	0.322
1	9	0.233	2	8	0.290
2	8	0.030	4	6	0.186
3	7	0.002	1	9	0.116
			5	5	0.059
			0	10	0.016
			6	4	0.010
			7	3	0.001

TABLE IX. Multi-basin QEI EDFs in the CO molecule at the DFT level (above a threshold of 0.030).

$n_{C(C)\cup V(C)}$	$n_{B^{C}_{C\text{-}O}}$	$n_{B^{O}_{C\text{-}O}}$	$n_{C(O)\cup V(O)}$	$p(S)$
2	0	3	5	0.110
3	0	3	4	0.096
2	0	4	4	0.084
3	0	2	5	0.083
2	0	2	6	0.070
3	0	4	3	0.050
4	0	2	4	0.037
2	1	3	4	0.036
2	1	2	5	0.035
2	0	5	3	0.032

Our second heterodiatomic is BeO. Recently, the nature of this and similar bonds formed by alkaline-earth atoms has raised renewed attention.[65,68] On one hand, it has been found that the heavier elements of the group, past Mg, use extensively their $(n-1)$d orbitals and can many times be considered as transition metals. This would be the case in the recently detected and widely studied late alkaline-earch octacarbonyl complexes.[68,69] On the other hand, several authors have also suggested that the bond between these elements and various electron-rich moieties like oxygen

or fluorine exhibits considerable multiple bond character.[65,68–70] In the specific case of BeO, and although it is recognized as a highly polar system, a bond order close to 3 has been proposed.[65]

Following a similar approach as in the previous cases, the QTAIM EDFs are shown in Fig. 6. The most relevant distribution is the $Be^{2+}O^{2-}$ doubly ionic structure, with a probability of 0.643 (see the Supporting Information, Section 3, for numerical details), followed by the singly ionic and the neutral distributions.

Four different basins appear in the ELF partition of BeO: the two core attractors C(Be) and C(O), the monosynaptic basin V(O), and the disynaptic basin V(Be,O). In Table X we observe that the most relevant distribution ($p = 0.276$) is the one where the disynaptic basin allocates 4 electrons and that it is only in the fourth entry of the Table that we find a bond valence populated with 2 electrons. Notice that this result is compatible with both a large multiple character of the bond and a very large polarity. This is possible after realizing (see Fig. 5) that most of the BeO bond valence domain belongs to the O QTAIM basin. Also relevant is the fact that the second and third entries of the Table depict back-and-forth one-electron transfers from the oxygen lone pairs to the BeO valence domain. These are the signature of electron sharing (i.e. covalency).[25]

TABLE X. Three-basin ELF EDFs in BeO at the DFT level (above a threshold of 0.020). In the case of O atom, core and monosynaptic basins are merged into a single fragment.

$n_{C(Be)}$	$n_{V(Be,O)}$	$n_{C(O)\cup V(O)}$	$p(S)$
0	4	4	0.276
0	3	5	0.231
0	5	3	0.172
0	2	6	0.098
0	6	2	0.051
1	3	4	0.034
1	4	3	0.027
1	2	5	0.021

Intersecting the QTAIM and ELF domains and performing a multi-basin EDF analysis yields the results contained in Table XI. It is now crystal clear that the BeO bond basin contains only a relevant number of electrons in its O sub-region, with a Be counterpart that is mostly empty. We believe that these data explain how two seemingly contradictory results are perfectly compatible

after all. A QTAIM analysis provides a highly charged system consistent with a Be^{2+} cation. Modern molecular orbital analyses do not deny this high polarity, but focusing on a one-electron picture they point to a BeO bond with considerable multiple character. The ELF picture leads to an interesting BeO bond basin that harbors many more than 2 electrons, and our final QEI picture tells us that these are electrons (some of them necessarily engaging in π interactions) that belong almost exclusively to the O basin. The final picture of BeO is that of a system with several bonding channels that are heavily polarized toward the O atom. Moreover, the several electron transfers between the $B^{Be}_{Be\text{-}O}$ and V(O) domains that appear in the first rows of Table XI also speak to the mobility of the valence electrons of oxygen. We also mention that using the so-called natural adaptive orbitals (NAdOs) we already reported a modest delocalization index equal to 0.72 but yet three bonding channels for BeO at a CAS(8,12) level.[71]

TABLE XI. Multi-basin QEI EDFs in the BeO molecule at the DFT level (above a threshold of 0.020).

$n_{C(Be)\cup V(Be)}$	$n_{B^{Be}_{Be\text{-}O}}$	$n_{B^{O}_{Be\text{-}O}}$	$n_{C(O)\cup V(O)}$	$p(S)$
0	0	4	4	0.195
0	0	3	5	0.181
0	0	5	3	0.108
0	0	2	6	0.084
0	1	3	4	0.069
0	1	4	3	0.051
0	1	2	5	0.044
1	0	3	4	0.029
0	0	6	2	0.028
1	0	4	3	0.021

We end by considering NO, a doublet radical in its ground state. As might have been expected for this slightly more complex case, Fig. 6 shows that a CAS description has some impact on the QTAIM probability distribution, hampering charge transfer and inverting the order of the two most likely structures seen at the DFT level. No further meaningful reordering is found in the rest of the structures, although the DFT results tend to overpopulate most of the multiple electron transfers.

The topology of the ELF function displays the five expected basins, with atomic lone pair regions and a single disynaptic V(N,O) domain. A three-basin EDF for it is found in Table XII at

the DFT level. A couple of points deserve mention. First, in consonance with what has been found in the previous heteroatomic examples, the V(N,O) bond basin (with an average of 2.10 electrons) has only two electrons in the most probable distributions but, simultaneously, the V(N) and V(O) domains exchange electrons quite easily. The multiple bond character of these interactions has then to be searched among the electrons that the ELF associates to atomic monosynaptic domains. Secondly, the unpaired electron is seen to reside mostly on the atomic lone pair regions. This is the expected behavior, although our data also clarify that this electron is quite delocalized, being found both on the oxygen and nitrogen ends.

TABLE XII. Three-basin ELF EDFs at DFT level of theory in the NO system (above a threshold of 0.030).

$n_{\mathrm{C(N)}\cup\mathrm{V(N)}}$	$n_{\mathrm{V(N,O)}}$	$n_{\mathrm{C(N)}\cup\mathrm{V(N)}}$	$p(S)$
4	2	5	0.151
3	2	6	0.107
3	3	5	0.098
4	3	4	0.092
4	1	6	0.091
5	2	4	0.079
5	1	5	0.071
3	1	7	0.046
3	4	4	0.040

The QEI partitioning adds further resolution to this analysis. In Table XIII we consider four fragments: $\mathrm{B}^{\mathrm{N}}_{\mathrm{N\text{-}O}}$ and $\mathrm{B}^{\mathrm{O}}_{\mathrm{N\text{-}O}}$, and the union of the cores and monosynaptic valence domains for each of the N and O atoms, respectively. We confirm that QEI adds a *polarity* axis to the ELF decomposition or a *bond* axis to the QTAIM partition. When we divide the electrons of the disynaptic basin, for instance, into its atomic constituents, most times they get associated with V(O), keeping the N bond sub-basin empty. This is what happens with the first entry in the Table. However, given the small electronegativity difference between N and O, the participation of N in the bond is not negligible, and the second distribution shows one electron residing in each sub-region. Similarly, the next two distributions depict the case where, starting from the first entry, one of the electrons from $\mathrm{B}^{\mathrm{O}}_{\mathrm{N\text{-}O}}$ is transferred to the vicinity of O (with a probability of 0.062) or to the vicinity of N (0.049), once again in agreement with electronegativity arguments.

TABLE XIII. Multi-basin EDFs within the QEI framework in the NO molecule at the DFT level (above a threshold of 0.030).

$n_{\mathrm{C(N)}\cup\mathrm{V(N)}}$	$n_{\mathrm{B}^{\mathrm{N}}_{\mathrm{N\text{-}O}}}$	$n_{\mathrm{B}^{\mathrm{O}}_{\mathrm{N\text{-}O}}}$	$n_{\mathrm{C(O)}\cup\mathrm{V(O)}}$	$p(S)$
4	0	2	5	0.071
4	1	1	5	0.066
4	0	1	6	0.062
5	0	1	5	0.049
3	1	1	6	0.048
3	0	2	6	0.047
3	1	2	5	0.044
4	1	2	4	0.042
5	0	2	4	0.038
5	1	1	4	0.034
3	0	1	7	0.031

V. CONCLUSIONS

Electron distribution functions provide the link between traditional concepts used in the theory of chemical bonding, such as covalency, ionicity, bond-order, etc., and the spatial arrangement of electrons in molecular systems. So far, they have been successfully applied to several problems by using either the spatial partitioning provided by the QTAIM, the ELF or the lattice sites of Hubbard models. Here we generalize them to the domains appearing from the intersection of the QTAIM and ELF attraction basins (QEI). In doing so, each entity corresponding to an ELF basin, like the bond domain of a Lewis pair, is split into a set of regions associated to different atoms. This gives, for example, intuitive access to the asymmetric partitioning of the electrons of a pair to the atoms participating in the bond.

In addition to providing the fundamentals of the new methodology, in this study we have examined the chemical bonding in saturated hydrides of the 2^{nd}, 3^{rd}, and 4^{th} periods, as well as three heterodiatomics, BeO, CO, and NO, with varying multiple bond character using the EDF approach. We first applied the QTAIM and ELF topological partitions to illustrate the bonding regime in terms of electron distributions between atoms and Lewis entities, respectively. Next,

QEI revealed a more insightful representation of the systems, providing a detailed breakdown of the electrons residing in the ELF basins (representing chemical bonds) into atomic contributions. In our view, this introduces a new paradigm for investigating chemical bonds using real-space techniques. We envision potential applications, including oxidation state assignment, which is currently a topic of interest in the physical chemistry community that we hope to exploit shortly. We have also examined the effect of electron correlation by comparing, for selected systems, the result provided by HF, CASSCF and B3LYP calculations. As is often the case when examining standard EDFs in mainly single reference molecules at or near their equilibrium geometries, the differences were more quantitative than qualitative, although in some systems, including BH_3, AlH_3 and NO, the shape of the EDF is smoothly altered when going from the DFT to the CAS levels.

SUPPLEMENTARY MATERIAL

Supplemental material includes a discussion of the active spaces used in the CASSCF calculations (section S1), and Tables of all EDFs with different partitioning schemes and basin decompositions for the AH_n (S2) and additional systems (S3).

CONFLICTS OF INTEREST

There are no conflicts to declare.

ACKNOWLEDGEMENTS

The authors acknowledge the Spanish "Ministerio de Ciencia e Innovación" for financial support (Grant No. PID2021-122763NB-I00) and the "Fundación para el Fomento en Asturias de la Investigación Científica Aplicada y la Tecnología" (Grant No. IDI-2021-000054). D. B.-E. acknowledges the spanish FICyT for the predoctoral grant PA-23-BP22-168.

REFERENCES

[1]G. Frenking and S. Shaik, *The chemical bond* (Wiley-VCH Verlag, Weinheim, Germany, 2014).

[2]S. Shaik, D. Danovich, W. Wu, P. Su, H. S. Rzepa, and P. C. Hiberty, Nat. Chem. **4**, 195–200 (2012).

[3]S. Shaik, H. S. Rzepa, and R. Hoffmann, Angew. Chem. Int. Ed. **52**, 3020–3033 (2013).

[4]G. Frenking and M. Hermann, Angew. Chem. Int. Ed. **52**, 5922–5925 (2013).

[5]P. Hobza and J. Řezáč, Chem. Rev. **116**, 4911–4912 (2016).

[6]S. Shaik, D. Danovich, J. M. Galbraith, B. Braïda, W. Wu, and P. C. Hiberty, Angew. Chem. Int. Ed. **59**, 984–1001 (2019).

[7]K. Ruedenberg, Rev. Mod. Phys. **34**, 326–376 (1962).

[8]S. Kurth and J. P. Perdew, Int. J. Quantum Chem. **77**, 814–818 (2000).

[9]L. Reuter and A. Lüchow, Nat. Commun. **12**, 4820 (2021).

[10]R. Bader and M. Stephens, Chem. Phys. Lett. **26**, 445–449 (1974).

[11]A. D. Becke and K. E. Edgecombe, J. Chem. Phys. **92**, 5397–5403 (1990).

[12]H. Schmider and A. Becke, J. Mol. Struct.: THEOCHEM **527**, 51 (2000).

[13]M. Kohout, Int. J. Quantum Chem. **97**, 651 (2004).

[14]E. Cancès, R. Keriven, F. Lodier, and A. Savin, Theor. Chem. Acc. **111**, 373 (2004).

[15]O. M. Lopes, B. Braïda, M. Causà, and A. Savin, "Understanding maximum probability domains with simple models," in *Progress in Theoretical Chemistry and Physics* (Springer Netherlands, 2011) p. 173–184.

[16]M. Menéndez, Á. Martín Pendás, B. Braïda, and A. Savin, Comp. Theor. Chem. **1053**, 142–149 (2015).

[17]P. L. A. Popelier, "On quantum chemical topology," in *Applications of Topological Methods in Molecular Chemistry* (Springer International Publishing, 2016) p. 23–52.

[18]P. Ziesche, "Cumulant expansions of reduced densities, reduced density matrices, and green's functions," in *Many-Electron Densities and Reduced Density Matrices*, edited by J. Cioslowski (Springer US, Boston, MA, 2000) pp. 33–56.

[19]K. Wiberg, Tetrahedron **24**, 1083–1096 (1968).

[20]I. Mayer, Chem. Phys. Lett. **97**, 270–274 (1983).

[21]M. Giambiagi, M. S. de Giambiagi, and K. C. Mundim, Struct. Chem. **1**, 423–427 (1990).

[22]A. Martín Pendás, E. Francisco, and M. A. Blanco, Phys. Chem. Chem. Phys. **9**, 1087 (2007).

[23]A. Martín Pendás, E. Francisco, and M. A. Blanco, J. Chem. Phys. **127**, 144103 (2007).

[24]R. F. W. Bader, *Atoms in Molecules* (Oxford University Press, Oxford, 1990).

[25]Á. Martín Pendás and E. Francisco, ChemPhysChem **20**, 2722 (2019).

[26]J. L. Casals-Sainz, J. Jara-Cortés, J. Hernández-Trujillo, J. M. Guevara-Vela, E. Francisco, and Á. Martín Pendás, Chem.– Eur. J. **25**, 12169–12179 (2019).

[27]Y. Grin, A. Savin, and B. Silvi, "The elf perspective of chemical bonding," in *The Chemical Bond: Fundamental Aspects of Chemical Bonding* (Wiley, 2014) p. 345–382.

[28]G. Acke, S. De Baerdemacker, P. W. Claeys, M. Van Raemdonck, W. Poelmans, D. Van Neck, and P. Bultinck, Mol. Phys. **114**, 1392–1405 (2016).

[29]D. Van Hende, L. Lemmens, S. De Baerdemacker, D. Van Neck, P. Bultinck, and G. Acke, J. Comput. Chem. **43**, 457–464 (2022).

[30]R. Freccero, J. Hübner, Y. Prots, W. Schnelle, M. Schmidt, F. R. Wagner, U. Schwarz, and Y. Grin, Angew. Chem. Int. Ed. **60**, 6457–6461 (2021).

[31]S. Raub and G. Jansen, Theor. Chem. Acc. **106**, 223–232 (2001).

[32]E. Matito and M. Solà, Coord. Chem. Rev. **253**, 647 (2009).

[33]D. Ferro-Costas and R. A. Mosquera, J. Chem. Theory Comput. **9**, 4816 (2013).

[34]D. Ferro-Costas, I. Pérez-Juste, and R. A. Mosquera, J. Comput. Chem. **35**, 978 (2014).

[35]T. Kato, Commun. Pure App. Math. **10**, 151–177 (1957).

[36]B. Silvi and A. Savin, Nature **371**, 683–686 (1994).

[37]V. Polo, J. Andrés, S. Berski, L. R. Domingo, and B. Silvi, J. Phys. Chem. A **112**, 7128–7136 (2008).

[38]J. Munarriz, E. Velez, M. A. Casado, and V. Polo, Phys. Chem. Chem. Phys. **20**, 1105–1113 (2018).

[39]J. Andrés, S. Berski, and B. Silvi, Chem. Commun. **52**, 8183–8195 (2016).

[40]A. Savin, A. D. Becke, J. Flad, O. K. Andersen, H. Preuss, and H. G. von Schnering, Angew. Chem. **30**, 409 (1991).

[41]A. Savin, O. Jepsen, J. Flad, O. K. Andersen, H. Preuss, and H. G. von Schnering, Angew. Chem. Int. Ed. Engl. **31**, 187 (1992).

[42]P. W. Ayers, J. Chem. Sci. **117**, 441 (2005).

[43]J. F. Dobson, J. Chem. Phys. **94**, 4328 (1991).

[44]B. Silvi, J. Phys. Chem. A **107**, 3081 (2003).

[45]E. Matito, B. Silvi, M. Duran, and M. Solà, J. Chem. Phys. **125**, 024301 (2006).

[46]E. Francisco, Á. Martín Pendás, and M. A. Blanco, J. Chem. Phys. **126**, 094102 (2007).

[47]E. Francisco, Á. Martín Pendás, and M. A. Blanco, Comput. Phys. Commun. **178**, 621–634 (2008).

[48]Á. Martín Pendás, E. Francisco, and M. A. Blanco, J. Phys. Chem. **111**, 1084 (2007).

[49]A. D. Becke, J. Chem. Phys. **98**, 1372 (1993).

[50]M. J. Frisch, G. W. Trucks, H. B. Schlegel, G. E. Scuseria, M. A. Robb, J. R. Cheeseman, G. Scalmani, V. Barone, G. A. Petersson, H. Nakatsuji, X. Li, M. Caricato, A. V. Marenich, J. Bloino, B. G. Janesko, R. Gomperts, B. Mennucci, H. P. Hratchian, J. V. Ortiz, A. F. Izmaylov, J. L. Sonnenberg, D. Williams-Young, F. Ding, F. Lipparini, F. Egidi, J. Goings, B. Peng, A. Petrone, T. Henderson, D. Ranasinghe, V. G. Zakrzewski, J. Gao, N. Rega, G. Zheng, W. Liang, M. Hada, M. Ehara, K. Toyota, R. Fukuda, J. Hasegawa, M. Ishida, T. Nakajima, Y. Honda, O. Kitao, H. Nakai, T. Vreven, K. Throssell, J. A. Montgomery, Jr., J. E. Peralta, F. Ogliaro, M. J. Bearpark, J. J. Heyd, E. N. Brothers, K. N. Kudin, V. N. Staroverov, T. A. Keith, R. Kobayashi, J. Normand, K. Raghavachari, A. P. Rendell, J. C. Burant, S. S. Iyengar, J. Tomasi, M. Cossi, J. M. Millam, M. Klene, C. Adamo, R. Cammi, J. W. Ochterski, R. L. Martin, K. Morokuma, O. Farkas, J. B. Foresman, and D. J. Fox, "*Gaussian 16 Revision C.01*," (2016).

[51]F. Weigend and R. Ahlrichs, Phys. Chem. Chem. Phys. **7**, 3297 (2005).

[52]G. M. J. Barca, C. Bertoni, L. Carrington, D. Datta, N. De Silva, J. E. Deustua, D. G. Fedorov, J. R. Gour, A. O. Gunina, E. Guidez, T. Harville, S. Irle, J. Ivanic, K. Kowalski, S. S. Leang, H. Li, W. Li, J. J. Lutz, I. Magoulas, J. Mato, V. Mironov, H. Nakata, B. Q. Pham, P. Piecuch, D. Poole, S. R. Pruitt, A. P. Rendell, L. B. Roskop, K. Ruedenberg, T. Sattasathuchana, M. W. Schmidt, J. Shen, L. Slipchenko, M. Sosonkina, V. Sundriyal, A. Tiwari, J. L. Galvez Vallejo, B. Westheimer, M. Wloch, P. Xu, F. Zahariev, and M. S. Gordon, J. Chem. Phys. **152**, 154102 (2020).

[53]F. F. S. Noury, X. Krokidis, and B. Silvi, "*The Topmod package*," (1997).

[54]A. Echeverri, M. Gallegos, T. Gómez, Á. Martín Pendás, and C. Cárdenas, J. Chem. Phys. **158**, 174101 (2023).

[55]G. Rayner-Canham, *Descriptive Inorganic Chemistry*, 6th ed. (W.H. Freeman, New York, NY, 2013).

[56]E. Chamorro, P. Fuentealba, and A. Savin, J. Comput. Chem. **24**, 496 (2003).

[57]R. J. Gillespie, I. Bytheway, T.-H. Tang, and R. F. W. Bader, Inorg. Chem. **35**, 3954 (1995).

[58]E. A. Robinson and R. J. Gillespie, Inorg. Chem. **42**, 3865 (2003).

[59]R. J. Gillespie, S. Noury, J. Pilmé, and B. Silvi, Inorg. Chem. **43**, 3248 (2004).

[60]A. J. W. Thom, E. J. Sundstrom, and M. Head-Gordon, Phys. Chem. Chem. Phys. **11**, 11297 (2009).

[61]V. Postils, C. Delgado-Alonso, J. M. Luis, and P. Salvador, Angew. Chem. Int. Ed. **57**, 10525–10529 (2018).

[62]M. Kaupp, Angew. Chem. Int. Ed. **40**, 3534 (2001).

[63]B. Silvi, Phys. Chem. Chem. Phys. **6**, 256 (2004).

[64]G. Frenking, C. Loschen, A. Krapp, S. Fau, and S. H. Strauss, J. Comput. Chem. **28**, 117 (2007).

[65]L. Zhao, S. Pan, and G. Frenking, J. Chem. Phys. **157**, 034105 (2022).

[66]J. Pilme, B. Silvi, and M. E. Alikhani, J. Phys. Chem. A **109**, 10028 (2005).

[67]J.-M. Ducéré, C. Lepetit, B. Silvi, and R. Chauvin, Organometallics **27**, 5263 (2008).

[68]R. Liu, L. Qin, Z. Zhang, L. Zhao, F. Sagan, M. Mitoraj, and G. Frenking, Chem. Sci. **14**, 4872 (2023).

[69]Y.-q. Liu, M.-h. Wang, B. Yan, L. Li, S. Pan, Z.-h. Cui, and G. Frenking, Chem. Eur. J. **29**, e202300446 (2023).

[70]L. Qin, Y.-q. Liu, R. Liu, X. Yang, Z.-h. Cui, L. Zhao, S. Pan, S. Fau, and G. Frenking, Chem. Eur. J. , e202304136 (2024).

[71]J. L. Casals-Sainz, A. Fernández-Alarcón, E. Francisco, A. Costales, and Á. Martín Pendás, J. Phys. Chem. A **124**, 339–352 (2019).